Kai Guo
School of Chemical Engineering
and Technology,
Tianjin University,
Tianjin 300350, China
e-mail: guokai2016207@tju.edu.cn

Wei Xu
School of Chemical Engineering
and Technology,
Tianjin University,
Tianjin 300350, China
e-mail: xw1224@tju.edu.cn

Zhanbin Jia
School of Chemical Engineering
and Technology,
Tianjin University,
Tianjin 300350, China
e-mail: zhanbin.jia@tju.edu.cn

Wei Tan[1]
Professor
School of Chemical Engineering and
Technology,
Tianjin University,
Tianjin 300350, China
e-mail: wtan@tju.edu.cn

Investigation of Fluid-Elastic Instability in Tube Arrays at Low Mass Damping Parameters in Cross-Flow

Fluid-elastic instability (FEI) is the most dangerous vibration mechanism in tube arrays. As the research shows in the recent years, the mechanism of FEI turns to be clear, but threshold prediction in low mass damping parameter (MDP) tube arrays is still not accurate because of the complexity of the instability mechanism. In this work, computational fluid dynamics (CFD) simulation is first validated by comparison with the water tunnel experiments in four kinds of tube arrangements and then extended to two-phase flow to get more data in low MDP range. Using fluid force coefficients calculated by CFD simulation, unsteady modeling of the tube model is established and the critical velocities match well with experiment and CFD simulation results. The effect of tube arrangement and Reynolds number on the fluid force coefficients and the predicted critical velocity is studied according to the unsteady flow theory. The results show that instability critical velocity of the normal triangular array can be underestimated at MDP lower than 1. When the frequency ratio (streamwise direction to transverse direction) decreases to below 0.8 in the rotated triangular array, the streamwise instability occurs earlier than transverse instability. The methods and conclusions in this paper can be used in FEI analysis in both streamwise direction and transverse direction.
[DOI: 10.1115/1.4045022]

Introduction

Tube arrays in cross-flow are likely to vibrate coupling with the fluid, which may cause excessive displacements of the tubes. For a certain tube array, the main flow excitation mechanisms are as follows: vortex shedding, turbulence buffeting, and fluid-elastic instability (FEI) [1,2]. Vortex shedding would not be a problem unless the tube natural frequency is right in the lock-in region. Turbulence cannot be avoided through reasonable designs, and fretting wear damage caused by turbulence at the tube supports may take many years. However, FEI generally occurs very abruptly and can cause catastrophic failures in a short period of time [3].

Fluid-elastic instability may cause large vibration amplitudes when flow velocity exceeds the critical value (U_c) [4,5]. As such, many empirical models have been proposed for fluid-elastic instability [5,6] mainly in the transverse direction. The most widely used model is the quasi-static model proposed by Connors [7]. In this model, the critical gap flow velocity (U_c) in the gap is expressed as

$$\frac{U_c}{f_n d} = K\left(\frac{m\delta}{\rho d^2}\right)^a \tag{1}$$

where d is the tube diameter; f_n is the natural frequency of the structure, m is the tube mass per unit length; δ is the structural damping logarithmic decrement, and ρ is the fluid density. It represents a very simple relationship between reduced critical flow velocity $U_{cr}(U_c/f_n d)$ and the mass damping parameter (MDP) $m\delta/\rho d^2$.

Price and Païdoussis proposed the quasi-steady flow model, in which the fluid-elastic forces on a tube are expressed as functions of the tube motion consisting of lift and drag coefficients [8,9]. The flow redistribution model of Lever and Weaver assumed the tube as a single degree-of-freedom system vibrating at the natural frequency of the center tube [6,10].

However, the fluid force coefficients in quasi-steady flow model are assumed to be independent of many factors such as Reynolds number and reduced velocity Ur. The flow channel assumption of Weaver and Lever is not so compatible in some certain tube arrays in high turbulence flow. In the unsteady flow theory of Chen and Tanaka [11–14], the fluid forces are as functions of structure displacements, velocities, and accelerations. As more factors are considered in unsteady flow theory, more fluid force coefficients are needed.

Consider a group of tubes vibrating in a flow, as shown in Fig. 1. The axes of the tubes are parallel to one another and perpendicular to the x–y plane. The radius R of each tube is the same, and the fluid is flowing with a gap flow velocity. The displacement components of a tube j in the x and y directions are u_j and v_j, respectively. The motion-dependent fluid force components acting

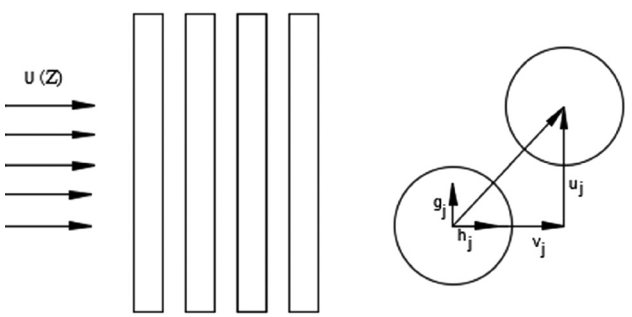

Fig. 1 Unsteady flow model

[1]Corresponding author.

Contributed by the Pressure Vessel and Piping Division of ASME for publication in the Journal of Pressure Vessel Technology. Manuscript received January 4, 2019; final manuscript received September 25, 2019; published online October 28, 2019. Assoc. Editor: Marwan A. Hassan.

on tube j in the x and y directions are, respectively, g_j and h_j given by the following equation:

$$g_j = -\rho\pi R^2 \sum_{k=1}^{n}\left(\alpha_{jk}\frac{\partial^2 u_k}{\partial t^2}+\sigma_{jk}\frac{\partial^2 v_k}{\partial t^2}\right) + \frac{\rho U^2}{\omega}\sum_{k=1}^{n}\left(\alpha'_{jk}\frac{\partial u_k}{\partial t}+\sigma'_{jk}\frac{\partial v_k}{\partial t}\right)+\rho U^2\sum_{k=1}^{n}\left(\alpha''_{jk}u_k+\sigma''_{jk}v_k\right) \quad (2)$$

$$h_j = -\rho\pi R^2 \sum_{k=1}^{n}\left(\tau_{jk}\frac{\partial^2 u_k}{\partial t^2}+\beta_{jk}\frac{\partial^2 v_k}{\partial t^2}\right) + \frac{\rho U^2}{\omega}\sum_{k=1}^{n}\left(\tau'_{jk}\frac{\partial u_k}{\partial t}+\beta'_{jk}\frac{\partial v_k}{\partial t}\right)+\rho U^2\sum_{k=1}^{n}\left(\tau''_{jk}u_k+\beta''_{jk}v_k\right) \quad (3)$$

where ρ is the fluid density; t is time; w is circular frequency of tube oscillations; α_{jk}, β_{jk}, σ_{jk}, and τ_{jk} are added-mass coefficients; α''_{jk}, β''_{jk}, τ''_{jk}, and σ''_{jk} are fluid stiffness coefficients; and α'_{jk}, β'_{jk}, σ'_{jk}, and τ'_{jk} are fluid damping coefficients.

These theories have ensured tube arrays in fluid-elastic stable condition when the equipment is designed by rules. However, there are still some problems to predict the threshold in whole range of mass damping parameters. Hassan proved that the fluid coefficient model (unsteady flow model and quasi-steady model) underestimates the threshold when MDP is smaller than 10, while the flow redistribution model can overestimate the threshold if MDP is greater than 10 [6]. But the reason was not explained in detail. The instability mechanism in this MDP range is quite complex. When MDP is larger than 1, the instability mechanism can be stiffness-controlled; otherwise, it can be damping-controlled [11]. In addition, the fluid force coefficient can be affected by Reynolds number and pitch ratio. However, it is not possible to define the Re values under which FEI occurs. It is necessary to find out the exact impact of Re on fluid-elastic instability critical velocity in different arrays.

The mechanism characteristic in the streamwise direction is still not clear enough. Fluid-elastic instability appears to occur in transverse direction before streamwise direction in most cases. However, the possibility of in-plane FEI in steam generators has been proved by the tube failures at San Onofre Nuclear Generating Station in California, U.S. [15]. Hirota et al. [16] studied a triangular array of tubes in air flow and concluded that the ratio of Connors' constant in the streamwise to that in the transverse direction is 1.5. Mureithi and coworkers [17,18] utilized quasi-steady model to predict in-plane fluid-elastic instability. They believed that frequency detuning plays an important role in streamwise fluid-elastic instability. Hassan and Weaver [4,19,20]provided more insight into this problem by numerical simulation, and the difference between streamwise and transverse directions of the natural frequency ratio could have some effects on the streamwise fluid-elastic instability in the rotated triangular array.

This paper presents fluid-elastic instability analysis with four kinds of tube arrays. Water tunnel experiments, unsteady flow theory modeling, and fluid–structure interaction (FSI) simulation on target tube arrays were performed. The FSI simulations are first verified by the experiments and then extended to two-phase flow to get more data at low MDP range. The effect of tube arrangement and Reynolds number was studied based on unsteady flow theory. In addition, the effect of the frequency ratio was also studied by FSI simulation. The overall goal of this research is to get a better prediction at low MDP and obtain some characteristics of both the streamwise and transverse instability.

2 Unsteady Theory Modeling

It is not easy to get the fluid force without experiments. In this work, the unsteady flow fluid force coefficients are obtained through computational fluid dynamics (CFD) simulation, the same method as Hassan. If a tube k is assumed to be excited in the x direction, its displacement in the x direction is given by

$$u_x = u\cos\omega t \quad (4)$$

The fluid force components acting on tube j in the transverse and streamwise directions are

$$F_L = \frac{1}{2}\rho U^2 c_{jk}\cos(\omega t + f_{jk})u \quad (5)$$

$$F_D = \frac{1}{2}\rho U^2 d_{jk}\cos(\omega t + \psi_{jk})u \quad (6)$$

where c_{jk} and d_{jk} are the fluid force amplitudes, and ϕ_{jk} and ψ_{jk} are the phase angles by which the fluid forces acting on tube j lead to the displacement of tube k

$$F_L = (\rho\pi R^2\omega^2\alpha_{jk}+\rho U^2\alpha''_{jk})u\cos\omega t - \rho U^2\alpha'_{jk}u\sin\omega t \quad (7)$$

$$F_D = (\rho\pi R^2\omega^2\tau_{jk}+\rho U^2\tau''_{jk})u\cos\omega t - \rho U^2\tau'_{jk}u\sin\omega t \quad (8)$$

In Eqs. (7) and (8)

$$\alpha''_{jk} = \frac{1}{2}c_{jk}\cos f_{jk} - \frac{\pi^3}{U_r^2}\alpha_{jk} \quad (9)$$

$$\tau''_{jk} = \frac{1}{2}d_{jk}\cos\psi_{jk} - \frac{\pi^3}{U_r^2}\tau_{jk} \quad (10)$$

$$\alpha'_{jk} = \frac{1}{2}c_{jk}\sin f_{jk} \quad (11)$$

$$\tau'_{jk} = \frac{1}{2}d_{jk}\sin\psi_{jk} \quad (12)$$

α'_{jk}, α''_{jk}, τ'_{jk}, and τ''_{jk} can be calculated from Eqs. (7)–(12). If tube k is excited in the y direction, force coefficients β'_{jk}, β''_{jk}, σ'_{jk}, and σ''_{jk} can be obtained in the same manner.

Fluid force coefficients depend on tube arrangement, tube pitch, oscillation amplitude, Reynolds number, and flow velocity. For a given tube array, fluid force coefficients are functions of oscillation amplitude, reduced flow velocity, and Reynolds number. According to the research of Chen, if oscillation amplitude is less than 70% of the gap, small-amplitude oscillations of the tubes due to other excitation sources are not expected to affect the threshold of fluid-elastic instability [13]. In this paper, when calculating the fluid force coefficients, 0.1 times of tube diameter d, which equals 0.25 times of the gap in this work, is selected to be the excitation amplitude. In a certain tube array, fluid coefficients can be treated as functions of U_r and Re. The structure function of tube array with n tubes can be depicted as

$$M\ddot{x}(t) + Kx(t) + C\dot{x}(t) = 0 \quad (13)$$

where $M = \{M_s+M_f\}$; $C = \{C_s+C_f\}$; $K = \{K_s+K_f\}$.

M_s is the mass matrix of structure, K_s is the structure stiffness matrix, C_s is the structure damping matrix, M_f is the added mass matrix, K_f is the fluid stiffness matrix, and C_f is the fluid damping matrix

$$K_f = \frac{1}{2}\rho U^2\begin{bmatrix}K_{xox} & K_{yox}\\ K_{xoy} & K_{yoy}\end{bmatrix} \quad (14)$$

$$C_f = \frac{1}{2}\rho DU\begin{bmatrix}C_{xox} & C_{xoy}\\ C_{yox} & C_{yoy}\end{bmatrix} \quad (15)$$

K_{xox}, K_{xoy}, K_{yox}, and K_{yoy} are the matrices of fluid stiffness coefficients, and C_{xox}, C_{xoy}, C_{yox} and C_{yoy} are the matrices of fluid

damping coefficients. It is not easy to separate function in one direction out because of coupling between the two directions. The coupling matrices such as K_{yox} and K_{xoy} can exist. If the effect was neglected or decoupled, the function could be translated only into the streamwise or transverse function.

3 Experiment Setup

3.1 Water Tunnel Test System. To study FEI characteristic of tube arrays, a set of water tunnel system with a new type of noncontact measurement was used, as shown in Fig. 2. Water pumped from the storage tank flowed through the regulating valve and the flow meter, then into the steady flow section, and returned to the tank at last. The centrifugal pump, the regulating valve, and the flow meter were connected to the control system. The flow control was realized by the upper computer interface. Test segment was 550 mm long with a cross section of 255 mm × 330 mm. The flow rate ranged from 0 to 300 m^3/h. The turbulence intensity of 5% could be set in this inlet region of the test section.

In the experiment, a noncontact measurement was implemented to obtain the vibration of the tube bundles. A high-speed camera was used to collect the data through a data acquisition window in the test section. The installation of the data acquisition setup was depicted in Fig. 3. The detailed procedure of visual image processing system and data processing method has been shown by Tan et al. [21].

3.2 Tubes Array and Tubes. The tube arrays consisted of two kinds of tubes: flexible ones and fixed ones. The flexible tubes were set in the central part of the test section. As shown in Fig. 4, flexible tubes were solid cantilever beams with a slender part (100 mm long) and a thick part (250 mm long). These kinds of tubes were widely used in FIV analysis. Fixed tubes were designed hollow rod with no slender part (Fig. 4(*b*)). Flexible tubes were made of aluminum alloy, while fixed tubes were made of steel. The frequency of the flexible tube in the air was 19.19±0.25 Hz, and the fixed tube was 140.6±2.9 Hz. Free vibration curve in the air of the flexible tubes is shown in Fig. 5.

There were four kinds of tube arrangement in this experiment containing normal square (90 deg), rotated square (45 deg), normal triangular (30 deg), and rotated triangular (60 deg). The pitch ratio was set as 1.28 and 1.4. Figure 6 shows the four kinds of tube arrays tested in the experiments. The tube response was obtained through visual image processing system method. Tube 13 in Fig. 6(*a*) and tube 12 in Figs. 6(*b*)–6(*d*) would be analyzed.

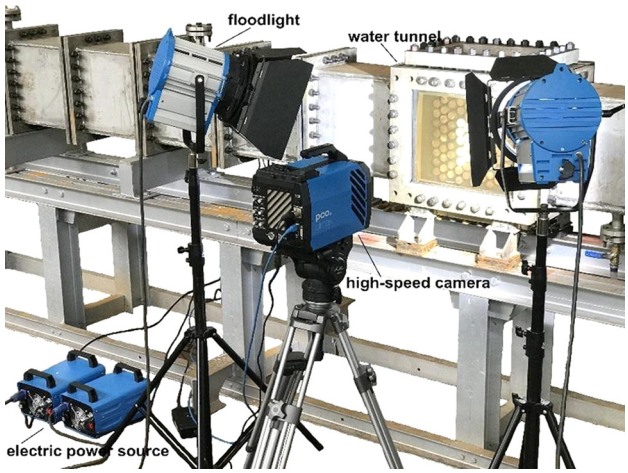

Fig. 3 Data acquisition system

4 Fluid–Structure Interaction Simulation

Fluid–structure interaction simulation can extend the results to larger MDP range below 10. Meanwhile, CFD results can also give more information about the flow field which can be helpful in FEI analysis. In this work, 2D-models were established to fulfill FEI study in water and two-phase flow condition.

4.1 Dynamic Tube Model. As is depicted in Fig. 7, the tube was treated as a rigid body and will vibrate only in two directions. The tube motion could only be translational in X and Y directions. It was based on a hypothesis that the tubes were excited in a statistical uniform state. The tube array was the same as in Fig. 6. The natural frequency can be controlled by setting the value of the stiffness (K_x and K_y) in each direction. The damping coefficient was set as 0.0002, which was obtained from the test in Sec. 3.2. The fluid dynamics model is described in detail by Hassan et al. [22]. FSI was handled by further casting the governing Reynolds average Navier–Stokes equations in an arbitrary Lagrangian–Eulerian form, which accommodated moving

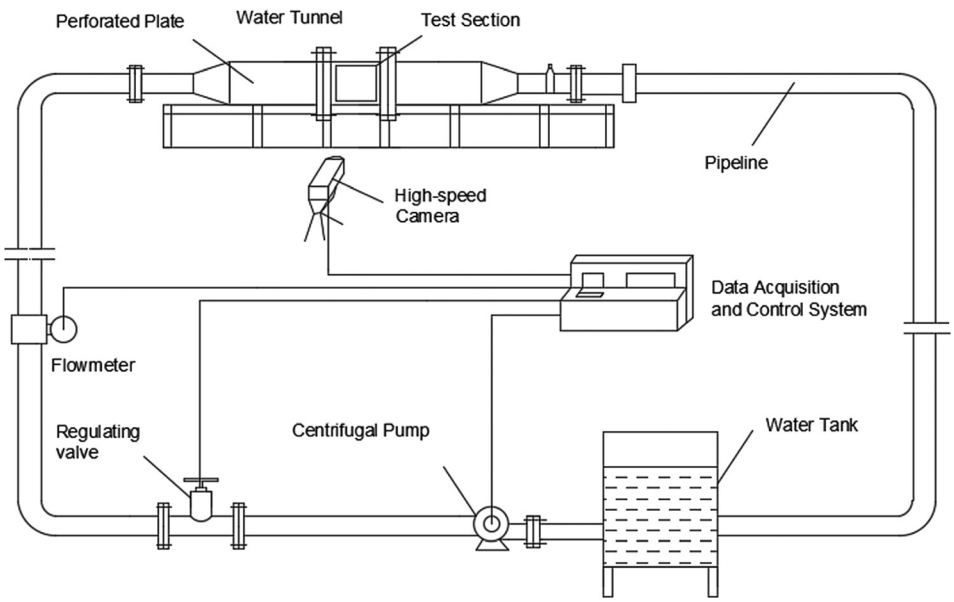

Fig. 2 Water tunnel system

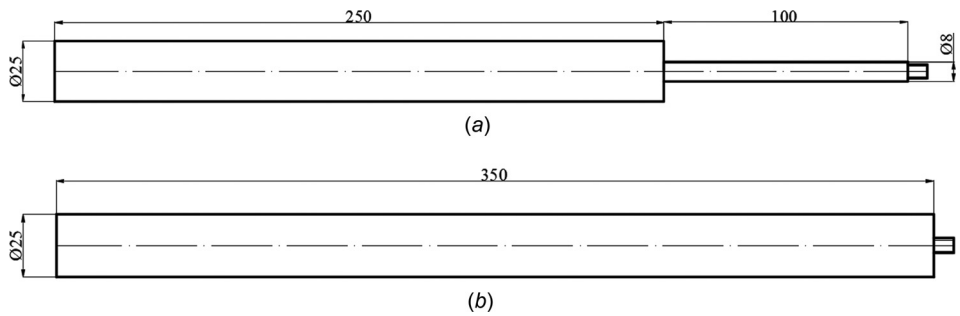

Fig. 4 Test tubes: (*a*) flexible tube and (*b*) fixed tube

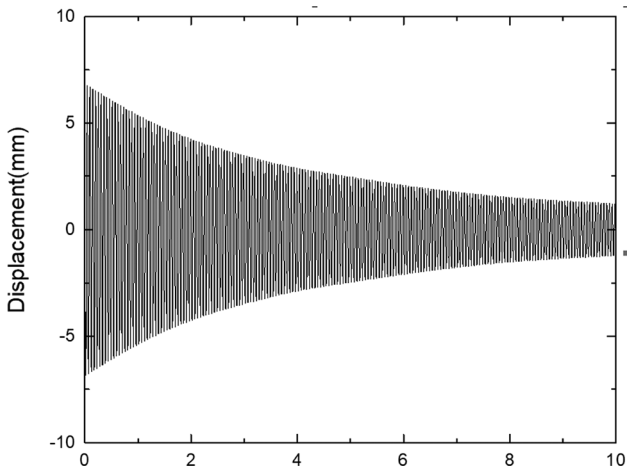

Fig. 5 Free vibration curve

boundaries and any subsequent deformation of the underlying dynamic mesh. To include the influence of turbulent mixing, the shear stress transport turbulence model is used. And the two-phase model was modeled with a homogeneous phase model in this work.

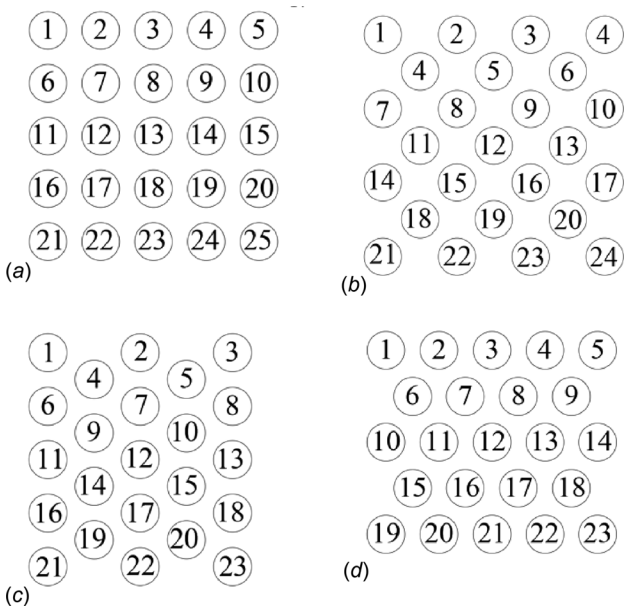

Fig. 6 Flexible tube arrays: (*a*) square array, (*b*) rotated square array, and (*c*) triangular array, and (*d*) rotated triangular array

4.2 Fluid-Elastic Instability Simulation. The tube arrays in this simulation were the same as those that had been depicted in the experiment setup. The fluids were set as water and air–water. The two-phase flow with void fractions of 0.5 and 0.8 was modeled with a homogeneous phase model in tube arrays with $P/d = 1.4$.

The tube responses were monitored. The models used in CFD simulation were shown in Fig. 8. The flexible tubes in the dashed line were tube arrays in Fig. 6. Average velocity inlet with 5% turbulence intensity and pressure outlet were adopted in this work. As the tube frequency is only 19 Hz, a time-step resolution based on T/n ($n > 200$) would be appropriate for the results. The inlet velocities range from 0.1 m/s until the velocity when fluid-elastic instability happened.

Independence of grids check was performed at inlet velocity $U = 0.3$ m/s in a normal square array. Lift coefficients C_L, drag coefficients C_d, and tube displacements were shown in Fig. 9. The model of 0.72×10^6 grids showed almost the same accuracy as 2.3×10^6 grids model. Considering the calculation scale and accuracy, the model of 0.72×10^6 grids were chosen as the calculation model to fulfill the study.

4.3 Fluid Force Coefficients Calculation. Same calculation models as Fig. 8 were built in CFD simulation in this section. Tube numbers in the unit tube cell is shown in Fig. 10. The fluid was chosen as water. The turbulence model, time–step, and grids were all the same as in the former section. Calculation of fluid force coefficients was needed to obtain the forces acting on the tubes. As is depicted previously, the central tube was excited as Eq. (6). The excitation amplitude u was 0.1d. The forces of the surrounding tubes were monitored.

According to the unsteady flow theory, fluid force coefficients were functions of Re and tube arrangement. Re was set as the same in one group of reduced flow velocities. In order to study the influence of Re, Re values were chosen as 12,500 and 18,250 based on gap velocities. The inlet velocities differed in various tube arrays, which were shown in Table 1.

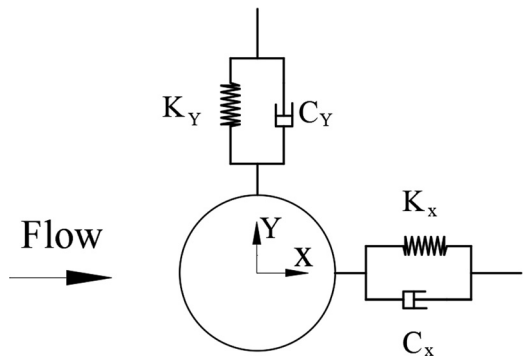

Fig. 7 Tube model

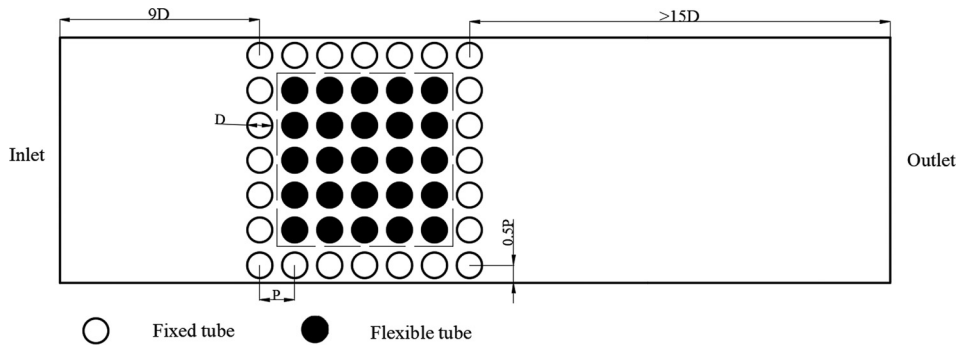

Fig. 8 Simulation tube arrays

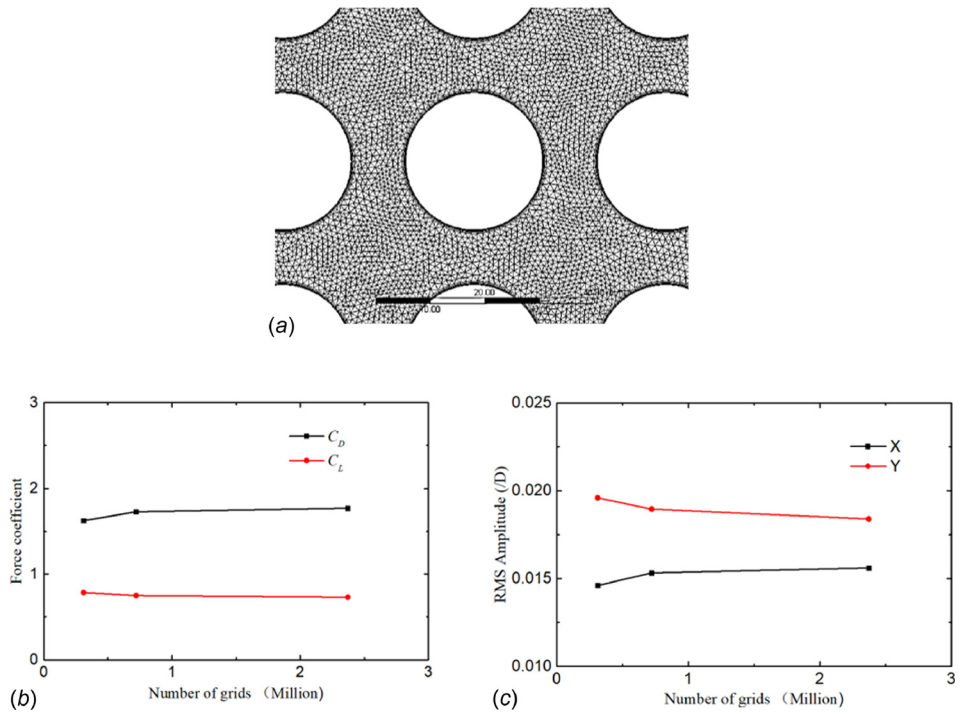

Fig. 9 Grids independence check: (*a*) local grid, (*b*) C_L and C_D, and (*c*) RMS displacements

5 Results and Discussion

5.1 Comparison of Experiment and Simulation

5.1.1 Fluid-elastic Instability Results. In this work, four kinds of tube arrangement with two pitch ratios P/d were tested in the water tunnel. Figure 11 shows the RMS value versus the flow gap velocity with $P/d = 1.4$. The rotated square array is the most likely to fall into an unstable state in water flow. But Nakamura showed fluid-elastic instability in the rotated square array is hard to occur in transverse direction according to his experiment in wind tunnel [23]. And in tube arrays with $P/d = 1.28$ and 1.4, fluid-elastic instability occurs in the transverse direction, which could be found in Figs. 11(*b*) and 12(*b*). It is obvious that damping-controlled instability can occur in the transverse direction in a rotated square

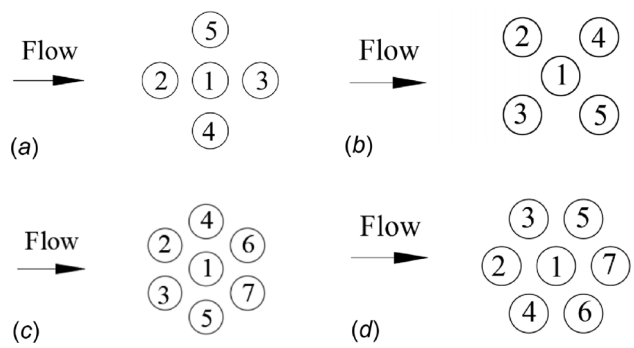

Fig. 10 Unit tube cell: (*a*) normal square array, (*b*) rotated square array, (*c*) normal triangular array, and (*d*) rotated triangular array

Table 1 Inlet velocity

Tube array	Reynolds number	Inlet velocity (m/s)
Normal square array	12,500	0.143
	18,250	0.214
Rotated square array	12,500	0.202
	18,250	0.303
Normal triangular array	12,500	0.143
	18,250	0.214
Rotated triangular array	12,500	0.171
	18,250	0.247

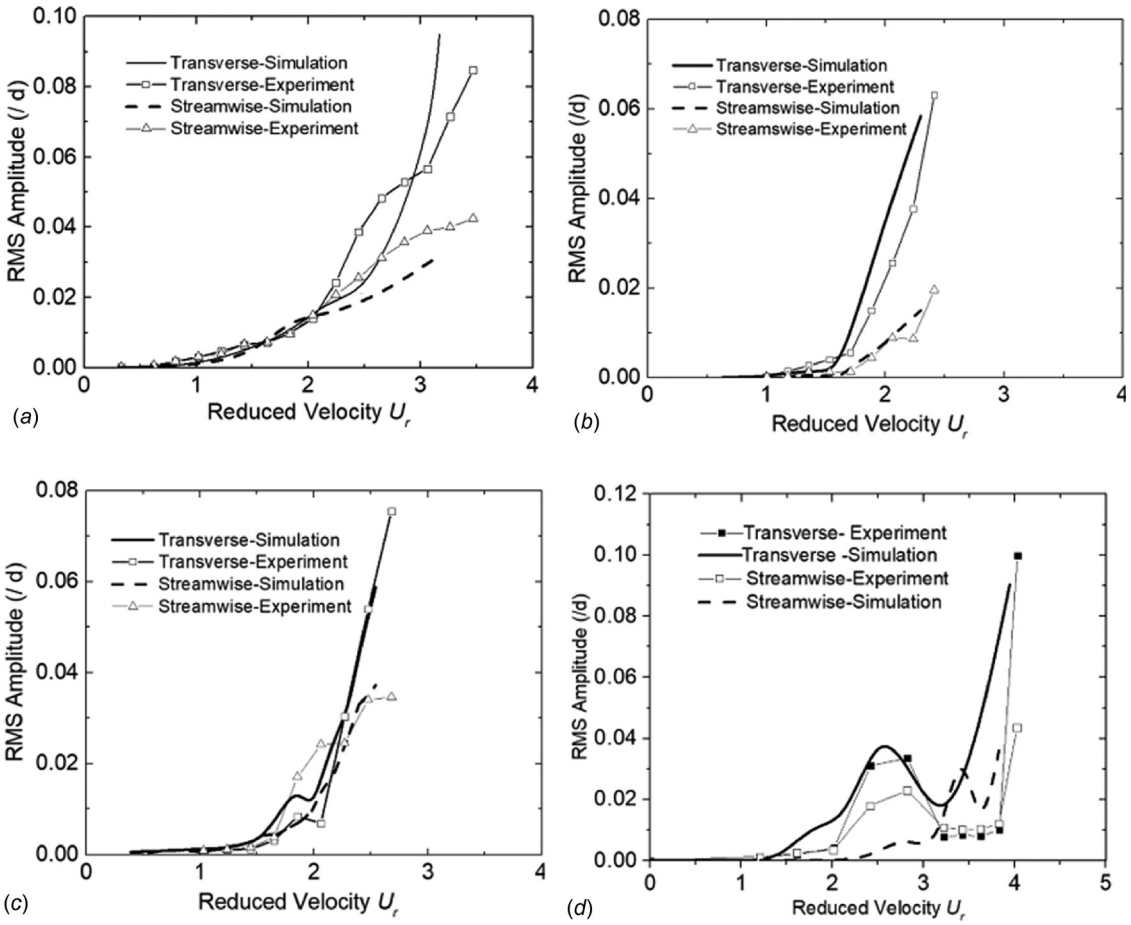

Fig. 11 RMS amplitude ($P/d = 1.4$): (*a*) normal square array, (*b*) rotated square array, (*c*) normal triangular array, and (*d*) rotated triangular array

array. This kind of tube array is easier to be unstable in water and more stable in air than other kinds of tube arrays.

In normal square arrays, the fluid-elastic instability is more likely to happen in the transverse direction than the streamwise direction. The trend is almost the same as the rotated triangular array. In triangular array (Fig. 11(*d*)), as the increase in reduced velocity, the RMS deplanement increased, then dropped a little, and increased rapidly after U_r is higher than 3.2. This can be caused by vortex shedding and fluid-elastic instability together. The results of tube arrays with $P/d = 1.28$ are shown in Fig. 12. This phenomenon still exists but is not so significant. In the spectrum of experimental displacements of normal triangular array at $U_r = 2.5$ ($P/d = 1.4$) (Fig. 13), two obvious peaks could be found. The peak at about 15 Hz is the response frequency of FEI response and the peak at about 18 Hz is vortex shedding frequency. Therefore, in a triangular array, critical velocity can be influenced by vortex shedding when the tube bundles are not close-packed. The streamwise direction result shows almost the same trend but the amplitude is much lower than that of transverse direction.

The tubes tend to vibrate with the easiest mode. If the fluid-tube system natural frequencies of the streamwise and transverse directions are the same, the rotated square array and rotated triangular array is more likely to vibrate in the mode dominated in the streamwise direction than other tube arrays. The streamwise fluid-elastic instability can occur before that in the transverse direction only in some special condition. The velocity vector maps in flexible tube array at low velocity (Re around 8000) are shown in Fig. 14. Vortex shedding obviously exists in all tube arrays. The flow paths in the rotated square array are almost the same in the streamwise and transverse direction. This can result in close critical velocities of two directions. The flow paths of the normal square array are almost straight and this makes it not easy to coupling in the streamwise direction.

In most of the tube arrays, critical velocity in tube bundles with pitch ratio $P/d = 1.4$ is larger than that of tube bundles with $P/d = 1.28$. Compared with relevant experiments, the results are reasonable. Many researchers have given suggestions on the selection of instability coefficient K with different pitch ratios, and critical velocity data in this work and other reported results [24–26] are depicted in Fig. 15.

The experimental results are close to the enveloping line of Chen [24]. The trend of the rotated triangular array and normal square array are almost the same. In the rotated triangular array, the critical velocity in this experiment is quite close to the enveloping threshold of Chen SS. Thus, the experimental results in this work are reliable and match well with the CFD simulation results.

More FSI simulations of tube arrays with $P/d = 1.4$ in two-phase flow were conducted, and the critical velocity is shown in Table 2. Streamwise instability occurs only in the rotated triangular array and the rotated square array in air–water flow of 0.8 void fraction. The critical velocity in the rotated square array is larger than that in the rotated triangular array. The time-domain displacements are shown in Fig. 16, in which a stable phase coupling was performed in the streamwise direction. Another information is that the mass damping parameters are all larger than 1, which means the instability can be stiffness controlled.

5.1.2 Fluid Force Coefficients. The results presented in this section are based on CFD simulations conducted over a range of reduced velocities between 0.1 and 100 using the same Reynolds number with relevant works of literature. Comparison with the

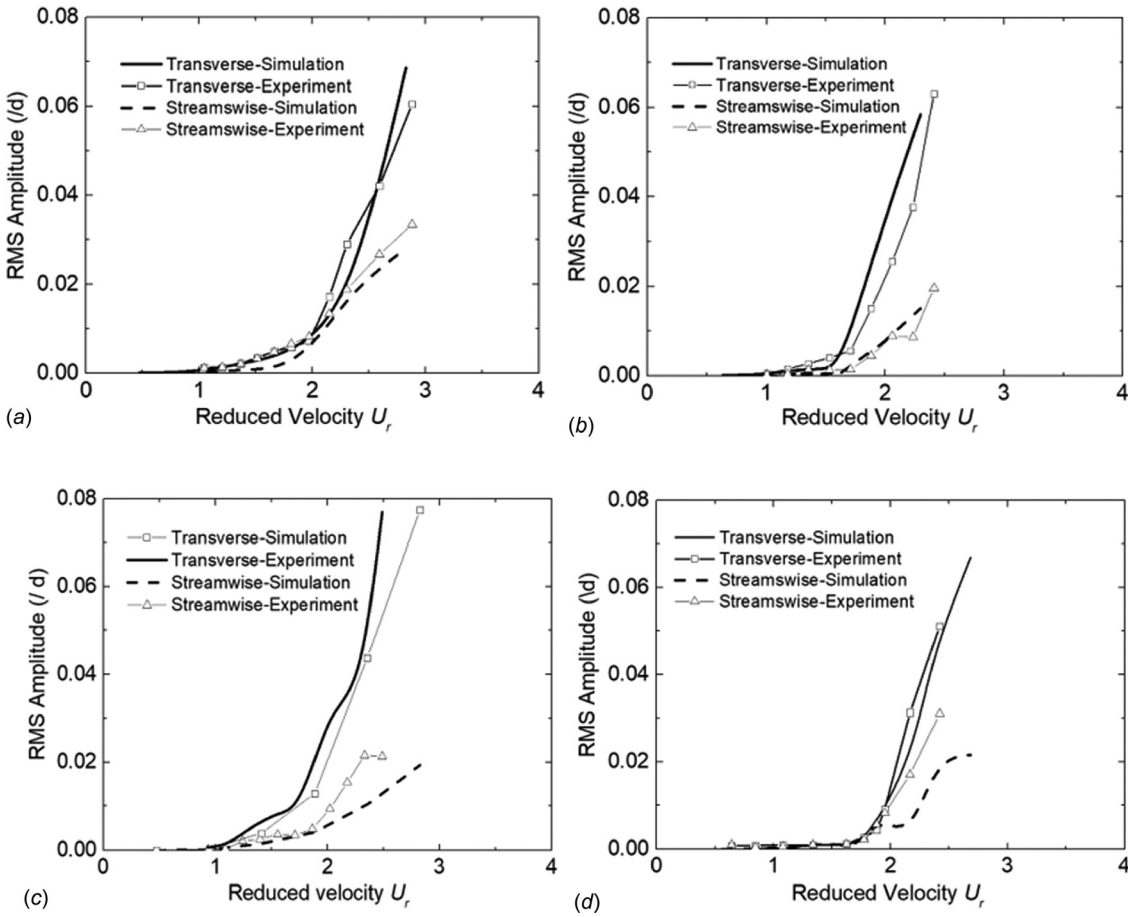

Fig. 12 RMS amplitude ($P/d = 1.28$): (*a*) normal square array, (*b*) rotated square array, (*c*) normal triangular array, and (*d*) rotated triangular array

experimental results of Tanaka and Chen are shown in Fig. 17 [13].

The experiments of Tanaka and Chen were carried out at $P/d = 1.375$, while the simulation was 1.4 in this work, which can be very close. The simulation trend matches well with the experimental data of Chen and Tanaka. In the MDP range around 5, the simulation results seem to have some differences with the reported experiments, which may result from the difference of P/d. When U_r is greater than 20, the stiffness coefficients and damping coefficients are almost independent of U_r. This can be found in both in-line and staggered tube arrays.

Therefore, more attention has been paid in the region $U_r < 20$ in this work. The coefficient data, as a function of the reduced flow velocity U_r, were then utilized to predict the stability threshold as a function of the mass damping parameter. The predicted results match well with the average trend of experimental data in both inline and staggered tube arrays. In Fig. 18(*a*), the predicted threshold is close to the lowest value of the experimental data of in-line array. The changing trend of stability threshold is well predicted in Fig. 18(*b*) by the data in this work in a staggered array. On the whole, the simulation and the experimental results agree quite well.

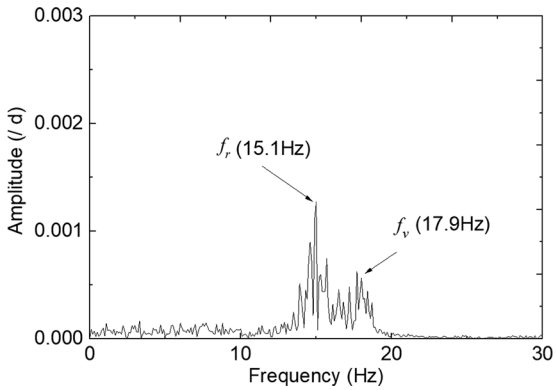

Fig. 13 Experimental spectrum of tube displacements

5.2 Effect of Reynolds Number. In Fig. 19, the simulation fluid force coefficients are compared with the experimental data [27,28]. It can be found that Re has a negative effect on fluid force coefficients, which has also been proved by Hassan et al. [22] and Chen et al. [27]. Higher Reynolds number results in lower values of the fluid force coefficients. As the increase in reduced velocity, the fluid force coefficient decreases sharply with the reduced velocity from 0 to 5. In Fig. 19(*a*), pitch ratio P/d of the square arrays herein is 1.4, which is almost the same as the experiment of Chen. With the increase in Re in the lower U_r region, the max value of damping coefficients increases and then drops to a very low value. When U_r is lower than 2, a little difference trend of damping coefficients can be found between the results of this work and Chen. Meanwhile, it matches well with the data of Tanaka.

In triangular array (Fig. 19(*b*)), the damping coefficients follow the same trend of the square array. The change of the damping coefficients at these two Re values is not as large as the former although the amplitude of Re variation is much larger. When it comes to the stiffness coefficients, the conclusion can also be found in Figs. 19(*c*) and 19(*d*).

The predicted critical velocity based on unsteady flow theory as the function of MDP, shown in Fig. 20, fits well with the trend of the reported experimental data and the results from CFD and water tunnel test in this work. The data point from this work with MDP lower than 1 is the result of water tunnel test, while the other data point in this work is FSI simulation results. The reported experiments are conducted under different P/d and Reynolds numbers. The data points of this work are with $P/d = 1.4$, and the Reynolds numbers vary from 10,000 to 20,000. The predicted critical velocity matches well with data in this work and fits well with the average trend of the reported data.

As is discussed by Tanaka, the effect of damping term mainly dominates in lower mass damping area which results in a turning of the line [11,28]. The stiffness effect will be dominant as the MDP increases. In Fig. 20, as the increase in Reynolds numbers, the turning point becomes lower. Therefore, the higher Reynolds number can result in the earlier dominant trend of stiffness effect. The increase in Reynolds number can have a positive effect on stiffness effect.

In Fig. 20(*a*), the predicted critical velocity is lower than the data point when mass damping parameters are lower than 1 in this work in the normal square array. Although the Reynolds number is close to 18,500, the model underestimates the critical velocity. This is the same as the conclusion of Hassan et al. [6]. In the normal triangular array, shown in Fig. 20(*b*), the trend of critical velocity change caused by Reynolds number is similar. The turning point can be found around 0.5, which is lower than the normal square array.

As is mentioned in the former part, the streamwise instability is easier to occur at MDP higher than 1. That means as the effect of stiffness term becomes larger, the streamwise instability is more likely to occur. If the MDP is lower than 1, as the fluid damping effect is more significant, higher Re value at the threshold can be expected. In turn, the critical velocity in streamwise direction can be much higher than the transverse direction.

In Fig. 21, fluid force coefficients ($U_r = 5$) are shown as a function of Re. The damping fluid force coefficients are not stable when U_r is less than 5. The pattern of the change caused by Reynolds number is not as stable in a square array as in the triangular array. As shown in Fig. 22, with the increase in Reynolds number, the fluid stiffness coefficients turn to be a constant value. That means the effect of Re is lower, and the predicted critical velocities of two higher Re will be closer, which can be found in the result of Hassan.

5.3 Effect of Tube Arrangement. The fluid force coefficients can be affected by tube arrangement. The critical velocity as the function of MDP is shown in Fig. 23. Although the influence of tube arrangement could not be easily described, some trends agree well with the experimental results. The critical velocity in the rotated triangular array can be lower than the normal square and triangular array but will become higher as MDP increases. This agrees well with the data by CFD simulation and experiment in Table 2. The critical velocity in square tube arrays can be larger than the other tube arrays when MDP is below 1 but will become smaller when MDP is larger than 1.

The turn caused by the change of stiffness effect and damping effect can be easily defined in Fig. 23. The turning MDP point of the triangular array is around 0.5, which is the lowest while other arrays are around MDP value of 1. This was not mentioned in Hassan's results because more attention was paid in MDP range larger than 1.

The effect of Re on the predicted instability threshold based on unsteady flow theory has already been mentioned in many researches. But the exact effect of Reynolds number with the

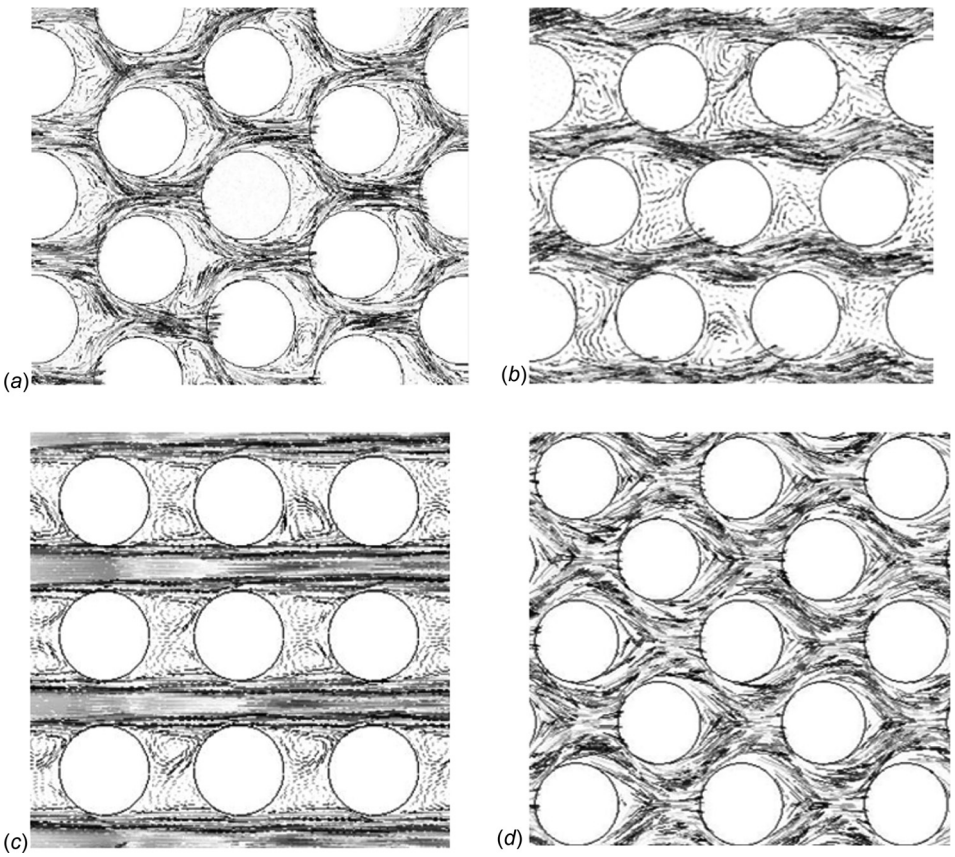

Fig. 14 Velocity vector in tube arrays: (*a*) normal triangle array, (*b*) rotated triangle array, (*c*) normal square array, and (*d*) rotated square array

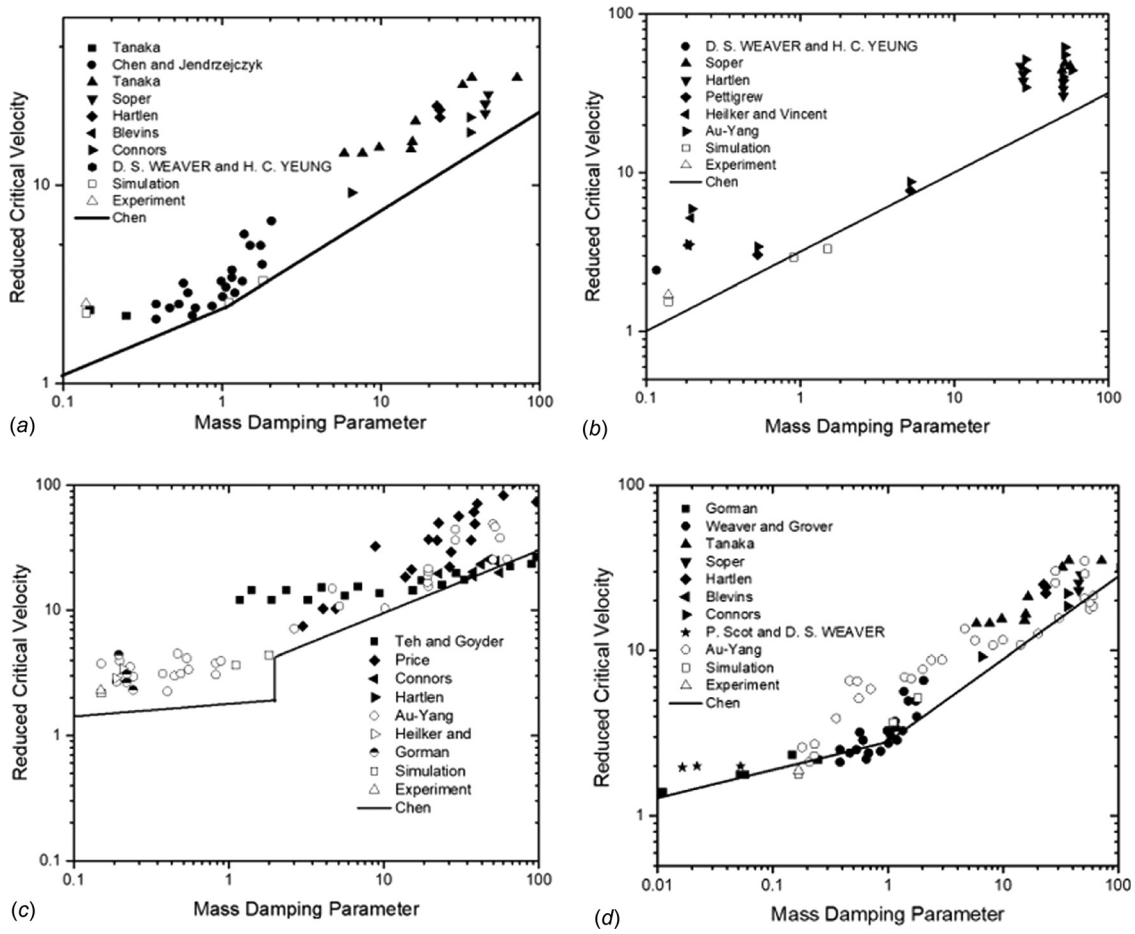

Fig. 15 Critical velocity comparison: (*a*) normal square array, (*b*) rotated square array, (*c*) normal triangle array, and (*d*) rotated triangle array

change of tube arrangements has not been discussed in detail. The unsteady modeling results of the tube arrays, reported experimental results, as well as the recommended threshold of Chen are shown in Fig. 24.

Compared with the experimental results, the critical velocity prediction of unsteady modeling matches well with the experimental and simulation data. In all tube arrays, as the increase in Re, the predicted critical velocity will be higher, which has also been proved by many researchers. Meanwhile, the turning MDP point becomes lower as the increase in Reynolds number. It also means the stiffness effect became larger as Re increases, although the effect of the damping terms on the stability is more pronounced at a low mass damping parameter.

The effect of Re change on critical velocity is more significant in the rotated square array than the square array. In the rotated triangular array, the effect of Re on critical velocity can be the most significant. As the Re of the data point in this work is about 18,500 and its MDP is lower than 1, unsteady modeling of critical velocity in the normal triangular array is the most underestimated.

As is depicted in Fig. 24(*a*), in the square array, the experimental data are quite close to Tanaka's predicted critical value. Predicted velocities under Re = 12,500 are lower than experimental and simulation values. The results of the rotated triangular array (Fig. 24(*d*)) are similar to the normal square array. The results predicted based on Re = 18,250 overvalued the critical velocity according to the experimental data and Chen's recommend value with mass damping parameters lager than 1. But in the two kinds of in-line array, the unsteady models do not underestimate the critical velocities too much when using data of corresponding Re.

The rotated square array is the only tube array with one recommended *K* value in the whole MDP region of Chen. In Fig. 24(*b*), it could be found that the recommended results are between the two unsteady modeling results based on different Re values. In Fig. 24(*c*), as the increase in Re, the turning point is lower in the triangular array. But the influence of Re on critical velocity is not as notable as that in the rotated triangular array. When mass damping parameters are lower than 1, the predicted critical velocities using fluid coefficients at Re = 18,250 are close to the experimental data, CFD simulation results, and Chen's enveloping line.

However, as the mass damping parameter is larger than 1, the results based on Re = 12,500 are closer to Chen's recommend value and experimental data. The critical velocity prediction in

Table 2 Critical velocity *P/d* = 1.4

		Critical velocity	
	Tube arrangement	Transverse	Streamwise
Water	Normal square	2.21	—
	Rotated square	1.97	—
	Normal triangular	3.85	—
	Rotated triangular	2.06	—
Air–water (0.5)	Normal square	2.58	—
	Rotated square	2.94	—
	Normal triangular	3.68	—
	Rotated triangular	3.69	—
Air–water (0.8)	Normal square	3.31	—
	Rotated square	3.32	8.84
	Normal triangular	5.16	—
	Rotated triangular	4.42	7.37

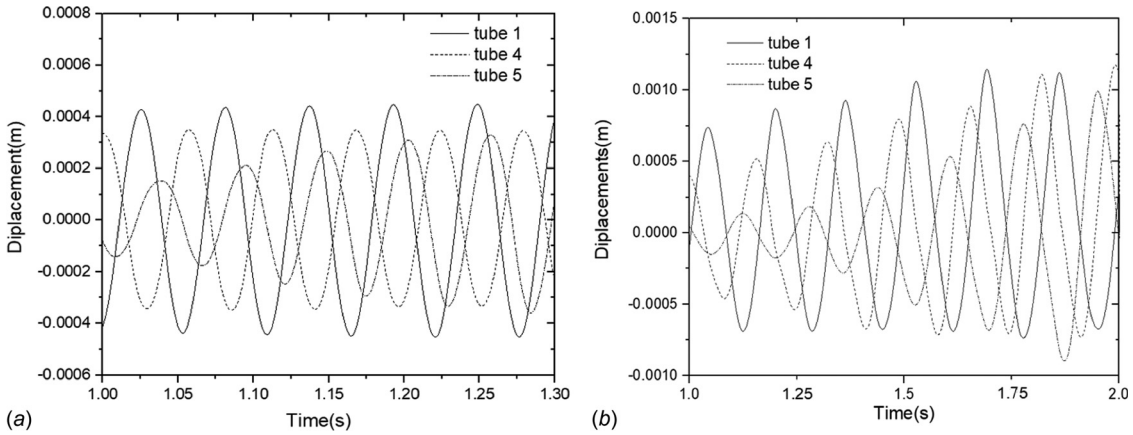

Fig. 16 Phase relationship for tube motion: (*a*) transverse response time trace ($U_r = 4.42$) and (*b*) streamwise response time trace ($U_r = 7.37$)

whole MDP range using unsteady flow theory requires selection of fluid force with properly high Re values, especially in low MDP range.

5.4 Effect of Frequency Ratio. In the practical heat exchanger, such as steam generators, the tube stiffness of two directions may not always be the same. This can cause some effects on the in-plane instability. Hassan and Weaver have studied the influence of frequency ratio f_s/f_t decrease on fluid-elastic instability in the streamwise direction in rotated triangular array [4]. As it is not easy to control the stiffness of tube in the water tunnel test, the CFD method was implemented to get the dynamic response of the square tube arrays and rotated triangular arrays with $P/d = 1.4$.

In water flow, no streamwise instability has been found in the two kinds of arrays. It has been widely known that fluid-elastic instability cannot occur in the streamwise direction in the normal square array. As is shown in Fig. 25, with the decrease in frequency ratio, the critical velocity in transverse direction increases first, but then tends to be stable when the frequency ratio dropped

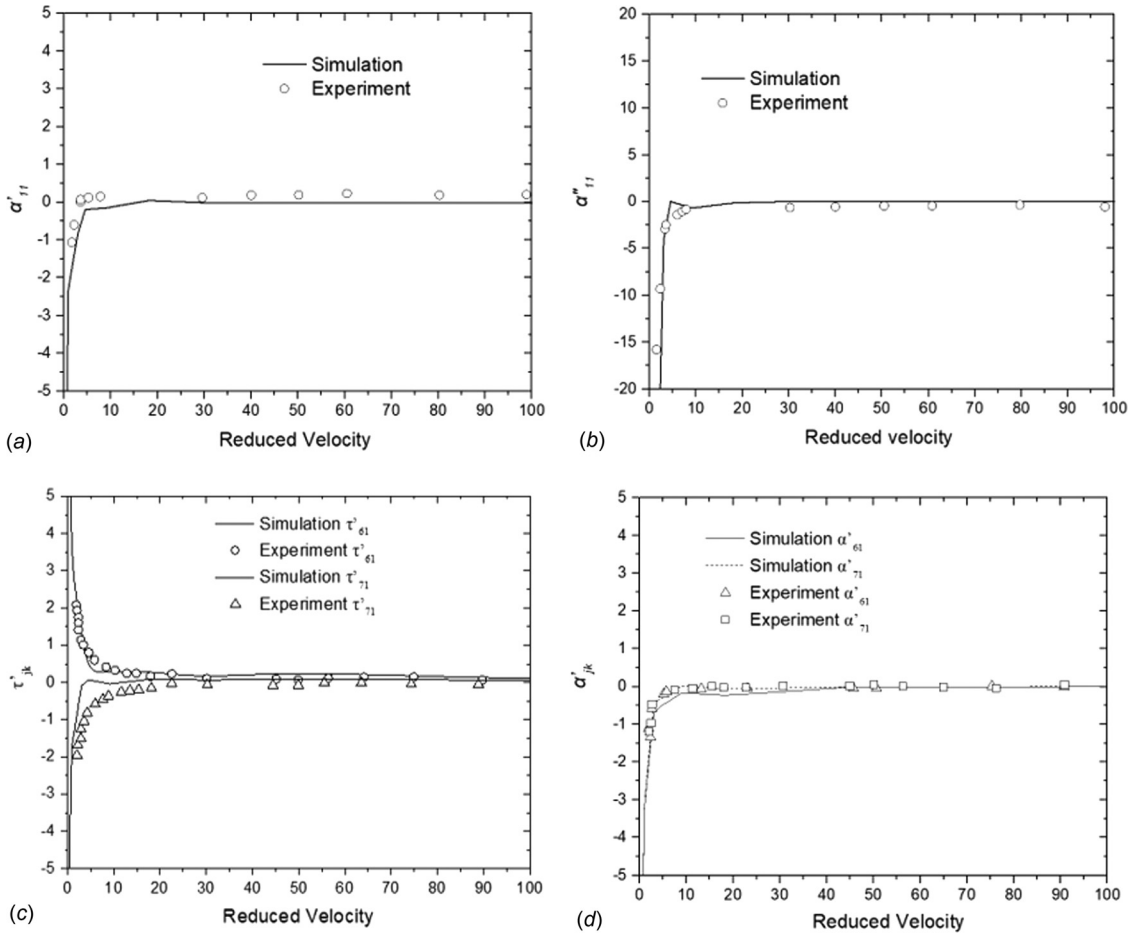

Fig. 17 Fluid force coefficients comparison: (*a*) damping coefficients in square array [13], (*b*) stiffness coefficients in square array [13], (*c*) and (*d*) damping coefficients in normal triangular array [13]

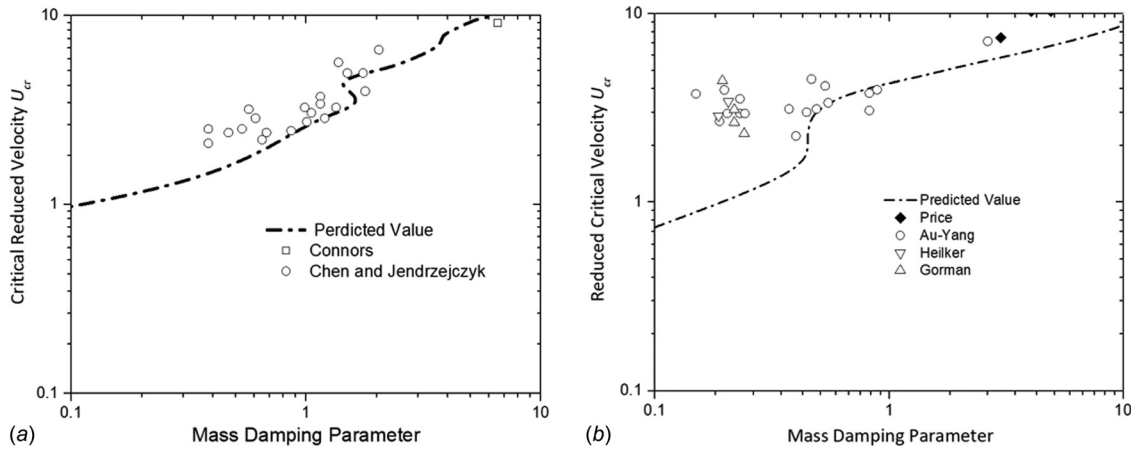

Fig. 18 Critical velocity as function of MDP: (*a*) in-line array and (*b*) staggered array

below 0.8. The difference of the frequency of tubes is proved to have a negative effect on the coupling of tubes by Tanaka et al. [28]. For a certain tube array, the input energy dissipated in streamwise direction can increase as the displacements became larger, which can result in less energy input in transverse direction. Therefore, the increase in critical velocity in transverse direction can also be explained. In the rotated triangular array, the increase in critical velocity is not so obvious as that in the normal square array.

In the two-phase flow, the critical velocity ratio as the function of frequency ratio f_s/f_t is shown in Fig. 26; the critical velocity in streamwise direction decreases as the frequency ratio drops, the trend of which is the same as Hassan and Weaver. The change of critical velocity can be quite complex in the frequency ratio range of 0.8–1.0, which has also been found by Hassan and Weaver [4] in the rotated triangular array by their time-domain model. When frequency ratio is lower than 0.8, the critical velocity ratios are higher than Hassan's. The reason can be the difference of mass

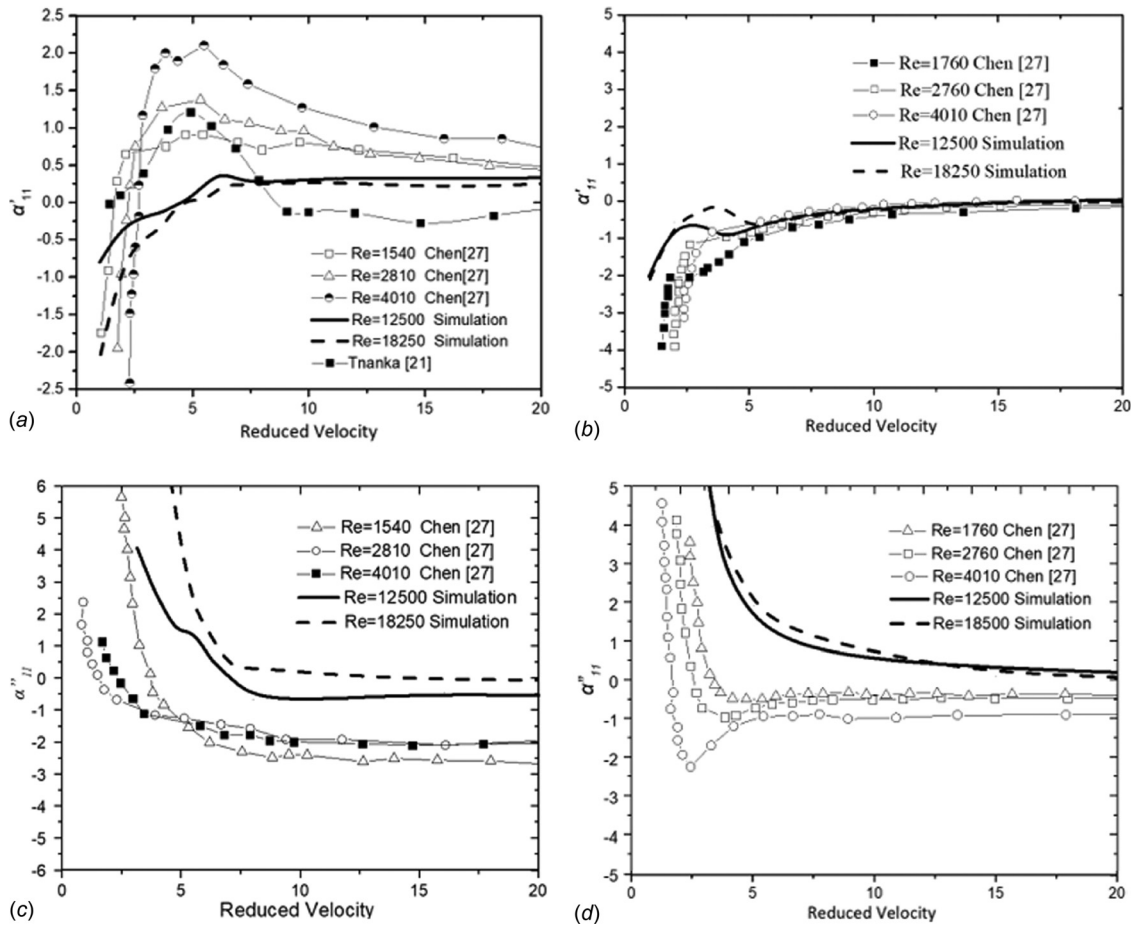

Fig. 19 Fluid force coefficients in tube arrays with different Re values: (*a*) damping coefficients—normal square array, (*b*) damping coefficients—triangular array, (*c*) stiffness coefficients—normal square array, and (*d*) stiffness coefficients—normal triangular array

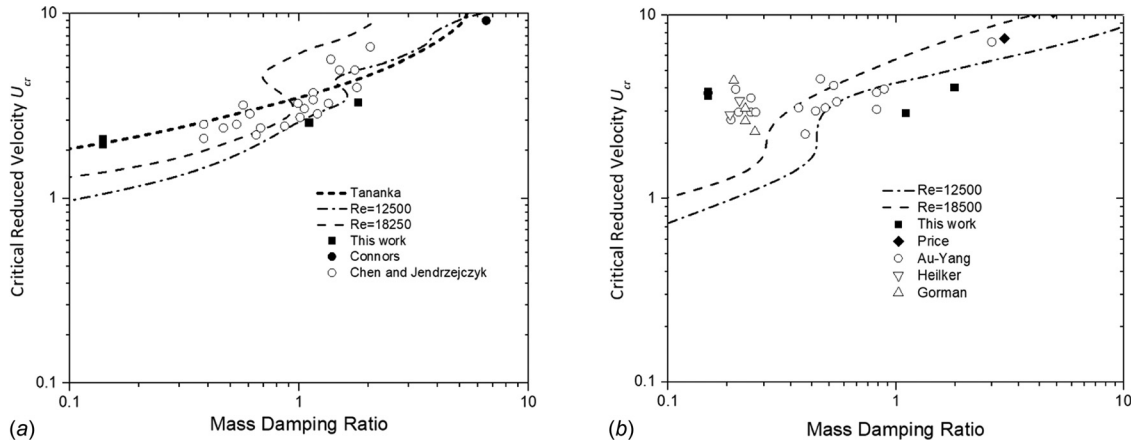

Fig. 20 Critical velocity with different Re values: (*a*) normal square array and (*b*) normal triangular array

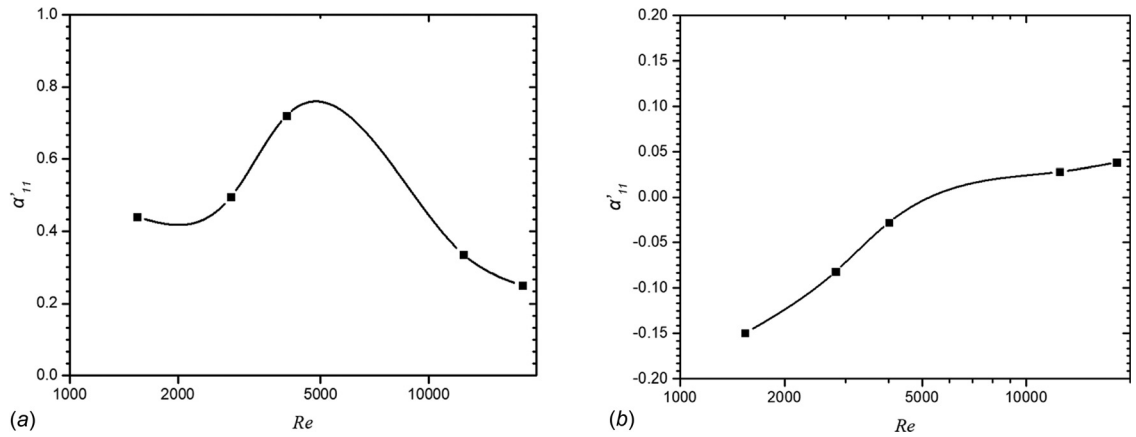

Fig. 21 Re effect on damping coefficients ($U_r = 20$): (*a*) normal square array and (*b*) normal triangular array

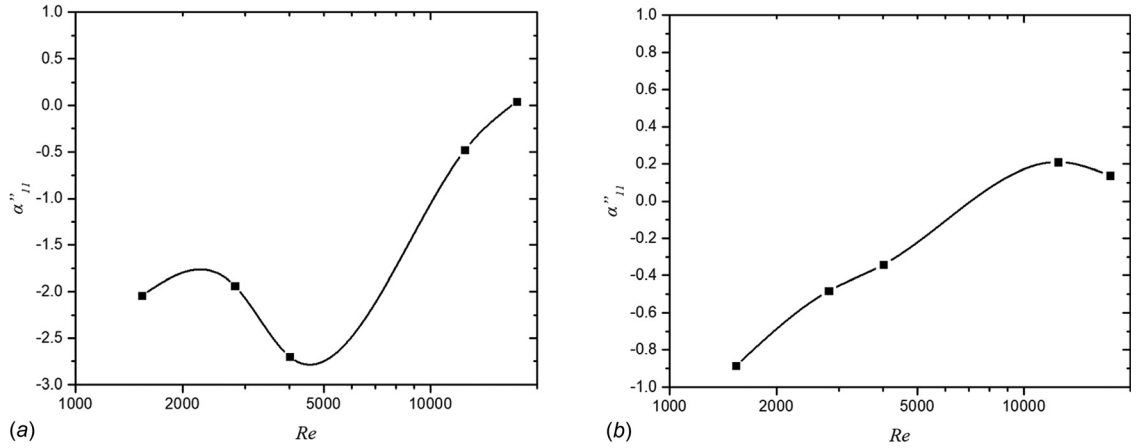

Fig. 22 Re effect on stiffness coefficients ($U_r = 5$): (*a*) normal square array and (*b*) normal triangular array

damping parameters between the two studies. As the MDP in his research is about 50, which is much larger than this work, the effect of system stiffness change can be more significant.

A single flexible tube in square and rotated triangular array cannot fall into streamwise instability [9,29]. In the research of Violette et al. [29], streamwise fluid-elastic instability cannot occur in the single flexible column tubes in the rotated triangular array. That means the effect between columns has an important effect on the streamwise FEI. In the rotated triangular array, the four adjacent tubes in the streamwise direction (tubes 3–6 shown in Fig. 10) can have some effects on the streamwise instability. The change of the force ratio may affect the vibration mode of tube unit cell with the seven tubes, and then the FEI in the streamwise direction would happen earlier than that in the transverse direction.

Conclusions

In this work, water tunnel experiments and CFD simulation were implemented to analyze fluid-elastic instability of four kinds

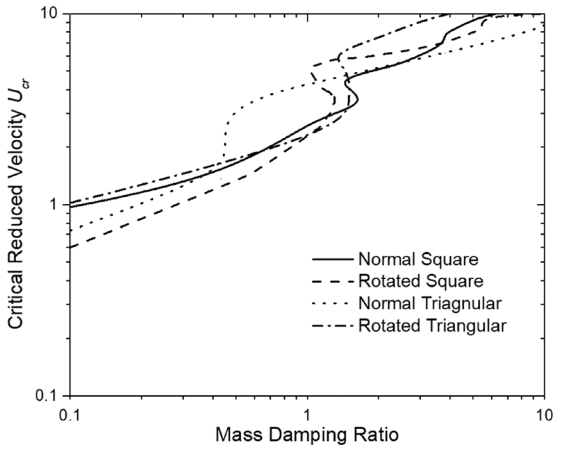

Fig. 23 Critical velocity of different tube arrangements (Re = 12,500)

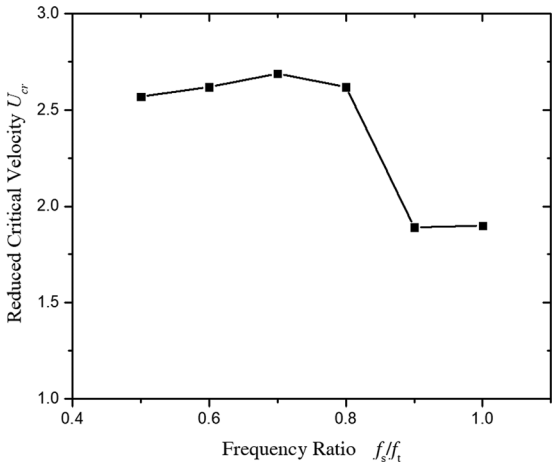

Fig. 25 Critical velocity in transverse direction

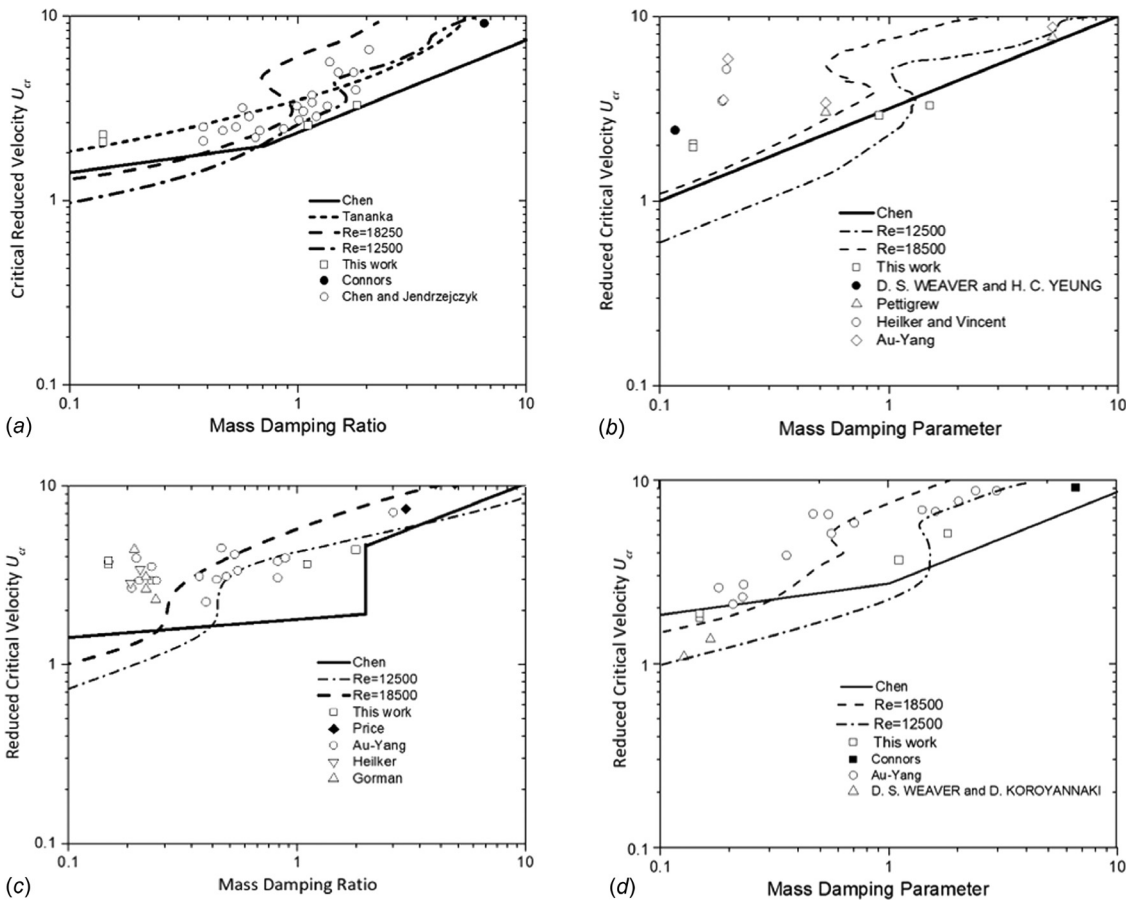

Fig. 24 Critical velocity prediction: (*a*) normal square, (*b*) rotated square, (*c*) normal triangular, and (*d*) rotated triangular

of tube arrangement with pitch ratio of 1.28 and 1.4. Using fluid force coefficients calculated by CFD simulation, unsteady flow modeling of FEI was established. The effect of Reynolds number and tube arrangement on the critical velocity and fluid force coefficients was analyzed. Some conclusions can be drawn as follows:

(1) When making prediction of a certain tube array, the application of fluid force coefficients under low Reynolds number can lead to the underestimation of critical velocity in low mass damping parameter tube arrays. In staggered arrays, when MDP is lower than 1, the critical threshold according the force coefficients of the corresponding Re can still be underestimated.
(2) As Reynolds number increases, the fluid force coefficients turn to decrease, and the increasing trend becomes gentle. Critical velocities predicted under two higher Reynolds number can be closer.
(3) Only in a rotated square array and rotated triangular array, streamwise instability was found in two-phase flow FSI simulation, when mass damping parameter is larger than 1. At this MDP, the stiffness-controlled instability can be more pronounced.

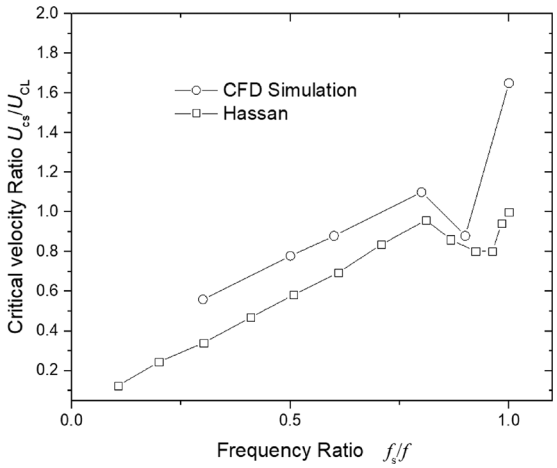

Fig. 26 Critical velocity ratio *Ucs*/*UcL*

(4) In the rotated triangular array, the transverse instability appears ahead of streamwise instability. However, as the frequency ratio decreases to below 0.8, streamwise instability critical velocity can be much lower, which can make the streamwise instability occur earlier than that of transverse direction. Through the comparison with reported data, this effect can be influenced by MDP.

Nomenclature

d = outside diameter, m
f_n = natural frequency, Hz
m = tubes' mass per unit length, kg/m
MDP = mass damping parameters
P = pitch
P/d = pitch ratio
Re = Reynolds number
U_c = critical velocity, m/s
U_{cr} = reduced critical velocity
Ur = reduced velocity
VIPS = visual image processing system
$\alpha, \beta, \tau, \sigma$ = added mass coefficient
$\alpha', \beta', \tau', \sigma'$ = damping coefficient
$\alpha'', \beta'', \tau'', \sigma''$ = stiffness coefficient
δ = logarithmic attenuation rate
ρ = density of fluid, kg/m^3

References

[1] Pettigrew, M. J., Taylor, C. E., Fisher, N. J., Yetisir, M., and Smith, B. A. W., 1998, "Flow-Induced Vibration: Recent Findings and Open Questions," Nucl. Eng. Des., **185**(2–3), pp. 249–276.
[2] Pettigrew, M. J., Carlucci, L. N., Taylor, C. E., and Fisher, N. J., 1991, "Flow-Induced Vibration and Related Technologies in Nuclear Components," Nucl. Eng. Des., **131**(1), pp. 81–100.
[3] Hassan, M., and Mohany, A., 2013, "Fluidelastic Instability Modelling of Loosely Supported Multispan U-Tubes in Nuclear Steam Generators," ASME J. Pressure Vessel Technol., **135**(1), p. 011306.
[4] Hassan, M., and Weaver, D. S., 2016, "Modelling of Streamwise and Transverse Fluidelastic Instability in Tube Arrays," ASME J. Pressure Vessel Technol., **138**(5), p. 0513041.
[5] Au-Yang, M. K., 1985, "Flow-Induced Vibration: Guidelines for Design, Diagnosis, and Troubleshooting of Common Power Plant Components," ASME J. Pressure Vessel Technol., **107**(4), pp. 326–334.
[6] Hassan, M., Rogers, R., and Gerber, A., 2010, "Time Domain Models for Damping-Controlled Fluidelastic Instability Forces in ***Multi*-Span Tubes With Loose Supports," ASME Paper No. FEDSM-ICNMM2010-30781.
[7] Connors, J. H. J., 1978, "Fluidelastic Vibration of Heat Exchanger Tube Arrays," ASME J. Mech. Des., **100**(2), pp. 347–353.
[8] Price, S. J., Païdoussis, M. P., and Al-Jabir, A. M., 1993, "Current-Induced Fluidelastic Instabilities of a Multi-Tube Flexible Riser: Theoretical Results and Comparison With Experiments," ASME J. Offshore Mech. Arct. Eng., **115**(4), pp. 206–212.
[9] Lever, J. H., and Weaver, D. S., 1986, "On the Stability of Heat Exchanger Tube Bundles—Part II: Numerical Results and Comparison With Experiments," J. Sound Vib., **107**(3), pp. 393–410.
[10] Lever, J. H., and Weaver, D. S., 1982, "A Theoretical Model for Fluid-Elastic Instability in Heat Exchanger Tube Bundles," ASME J. Pressure Vessel Technol., **104**(3), pp. 147–158.
[11] Tanaka, H., and Takahara, S., 1981, "Fluid Elastic Vibration of Tube Arraay in Cross Flow," J. Sound Vib., **77**(1), pp. 19–37.
[12] Chen, S. S., 1975, "Vibration of Nuclear Fuel Bundles," Nucl. Eng. Des., **35**, pp. 399–422.
[13] Chen, S. S., and Srikantiah, G. S., 2001, "Motion-Dependent Fluid Force Coefficients for Tube Arrays in Crossflow," ASME J. Pressure Vessel Technol., **123**(4), pp. 429–436.
[14] Tanaka, H., Takahara, S., and Ohta, K., 1982, "Flow-Induced Vibration of Tube Arrays With Various Pitch-to-Diameter Ratios," ASME J. Pressure Vessel Technol., **104**(3), pp. 168–174.
[15] Blevins, R. D., 2018, "Nonproprietary Flow-Induced Vibration Analysis of San Onofre Nuclear Generating Station Replacement Steam Generators to ASME Code Section III Appendix N," ASME J. Pressure Vessel Technol., **140**(3), p. 034502.
[16] Hirota, K., Morita, H., Hirai, J., Iwasaki, A., Utsumi, S., Shimamura, K., and Kawakami, R., 2013, "Investigation on in-Flow Fluidelastic Instability of an Array of Tubes," ASME Paper No. PVP2013-97163.
[17] Mureithi, N. W., Zhang, C., Ruël, M., and Pettigrew, M. J., 2005, "Fluidelastic Instability Tests on an Array of Tubes Preferentially Flexible in the Flow Direction," J. Fluids Struct., **21**(1), pp. 75–87.
[18] Olala, S., and Mureithi, N. W., 2017, "Prediction of Streamwise Fluidelastic Instability of a Tube Array in Two-Phase Flow and Effect of Frequency Detuning," ASME J. Pressure Vessel Technol., **139**(3), p. 031301.
[19] Hassan, M., and Weaver, D., 2017, "Pitch and Mass Ratio Effects on Transverse and Streamwise Fluidelastic Instability in Parallel Triangular Tube Arrays," ASME J. Pressure Vessel Technol., **139**(6), p. 061302.
[20] Chen, S. S., 1983, "Instability Mechanisms and Stability Criteria of a Group of Circular Cylinders Subjected to Cross-Flow—Part I: Theory," ASME J. Vib., Acoust., Stress, Reliab. Des., **105**(1), pp. 51–58.
[21] Tan, W., Li, Z., Wu, H., Wang, Y., Zhang, Y., Zou, J., and Zhu, G., 2018, "Experiment Study on Fluidelastic Instability of Tube Bundles Consisting of Different Frequency Tubes With Visual Image Processing System," ASME J. Pressure Vessel Technol., **140**(3), p. 031302.
[22] Hassan, M., Gerber, A., and Omar, H., 2010, "Numerical Estimation of Fluidelastic Instability in Tube Arrays," ASME J. Pressure Vessel Technol., **132**(4), p. 041307.
[23] Nakamura, T., and Tsujita, T., 2017, "Study on the Stream-Wise Fluidelastic Instability of Rotated Square Arrays of Circular Cylinders Subjected on Cross-Flow," ASME Paper No. PVP2017-65162.
[24] Chen, S. S., 1984, "Guidelines for the Instability Flow Velocity of Tube Arrays in Crossflow," J. Sound Vib., **93**(3), pp. 439–455.
[25] Weaver, D. S., and Fitzpatrick, J. A., 1988, "A Review of Cross-Flow Induced Vibrations in Heat Exchanger Tube Arrays," J. Fluids Struct., **2**(1), pp. 73–93.
[26] Au-Yang, M. K., Blevins, R. D., and Mulcahy, T. M., 1991, "Flow-Induced Vibration Analysis of Tube Bundles—a Proposed Section III Appendix N Nonmandatory Code," ASME J. Pressure Vessel Technol., **113**(2), pp. 257–267.
[27] Chen, S. S., Cai, Y., and Srikantiah, G. S., 1998, "Fluid-Damping-Controlled Instability of Tubes in Crossflow," J. Sound Vib., **217**(5), pp. 883–907.
[28] Tanaka, H., Tanaka, K., Shimizu, F., and Takahara, S., 2002, "Fluidelastic Analysis of Tube Bundle Vibration in Cross Flow," J. Fluids Struct., **16**(1), pp. 93–112.
[29] Violette, R., Pettigrew, M. J., and Mureithi, N. W., 2005, "Fluidelastic Instability of an Array of Tubes Preferentially Flexible in the Flow Direction Subjected to Two-Phase Cross Flow," ASME J. Pressure Vessel Technol., **128**(1), pp. 148–159.